Composites: Part A 100 (2017) 106–117

Contents lists available at ScienceDirect

Composites: Part A

journal homepage: www.elsevier.com/locate/compositesa

Dual modification of graphene by polymeric flame retardant and Ni $(OH)_2$ nanosheets for improving flame retardancy of polypropylene

Bihe Yuan [a,b], Yuan Hu [b,*], Xianfeng Chen [a,*], Yongqian Shi [c], Yi Niu [a], Ying Zhang [a], Song He [a], Huaming Dai [a]

[a] School of Resources and Environmental Engineering, Wuhan University of Technology, Wuhan 430070, China
[b] State Key Laboratory of Fire Science, University of Science and Technology of China, Hefei 230026, China
[c] College of Environment and Resources, Fuzhou University, Fuzhou 350116, China

ARTICLE INFO

Article history:
Received 1 March 2017
Received in revised form 5 April 2017
Accepted 14 April 2017
Available online 19 April 2017

Keywords:
A. Polymer-matrix composites (PMCs)
B. Thermal properties
D. Thermal analysis

ABSTRACT

To improve its dispersion and flame retardant efficiency, graphene oxide (GO) is dually modified with polymeric flame retardant and the nanomaterial with catalytic carbonation ability. Via the reactions between oxygen functional groups in GO and P—Cl groups in hexachlorocyclotriphosphazene, phosphazene-based flame retardant is grafted to GO. Due to the strong affinity of Ni^{2+} with NH_2 groups in this phosphazene flame retardant, the decoration of $Ni(OH)_2$ nanosheets on the graphene is facilitated. Transmission electron microscopy images confirm good dispersion and exfoliation state of graphene in polypropylene (PP) matrix. The incorporation of functionalized graphene oxide (FGO) results in the reduction of peak heat release rate, total heat release and smoke release of PP during the combustion. Flame mechanism of FGO is concluded according to the results of thermal decomposition and char analysis. This work provides a novel modification strategy for enhancing the dispersion and flame retardant efficiency of graphene.

1. Introduction

Since its successful isolation in 2004, graphene has attracted an enormous amount of attention in polymer composites due to its extraordinary physical properties. It is well-known that the dispersion of nanofillers in polymer matrix directly determines their enhancements in the physical properties of resultant composites. However, the intrinsically strong interactions between graphene nanosheets render them difficult to be well-dispersed in polymer, especially for non-polar polyolefin, such as polypropylene (PP). Numerous studies have confirmed that surface modification of graphene is important for enhancing its dispersion and compatibility within polymers [1,2]. Non-covalent and covalent modifications are the main functionalization methods for graphene. Non-covalent modification employs the weak interactions, such as π-π stacking and Van der Waals forces, between graphene and modifiers [1]. The most obvious merit for non-covalent modification is the preservation of original chemical structure of graphene [3]. However, covalent modification of graphene will produce additional defects, which may exert a negative influence on the mechanical and thermal properties of graphene and its resultant composites [3,4]. Despite the presence of this disadvantage, grafting graphene with polymer modifiers is more effective to improve its dispersion and achieve stronger load transfer efficiency [2].

Besides the aforementioned organic modification, functionalization of graphene with other nanomaterials has also been proven to be an effective approach to improve its dispersion in polymers [2,5]. Because of the presence of large specific surface area and residual functional groups, graphene has been used as a promising substrate for the loading of inorganic nanomaterials. In the graphene-based nanohybrid, the enhanced properties is achieved by the synergism between graphene and exogenous nanomaterials [6]. The residual oxygen-containing groups in graphene is a prerequisite for the tight immobilization of nanomaterials, due to the achievement of strong interactions [7]. Thus, the oxygen functional groups on graphene oxide (GO) play an important role in the immobilization and distribution of nanomaterials. These functional groups show strong affinity to metal ions and provide active immobilization sites for nanomaterials [7]. GO is highly thermally unstable and its oxygen moieties can be easily removed by heating or a variety of reagents [8]. Thus, this removal of oxygen functional

* Corresponding authors.
E-mail addresses: yuanhu@ustc.edu.cn (Y. Hu), cxf618@whut.edu.cn (X. Chen).

http://dx.doi.org/10.1016/j.compositesa.2017.04.012
1359-835X/

groups will exert an unfavorable influence on the anchoring of foreign nanomaterials. It is of great importance to modify the surface characteristic of graphene, providing more active sites for the loading of nanomaterials [7]. Similar to graphene, nanomaterials also have strong tendency to form agglomerates in polymer matrices. In the nanohybrids, the deposited nanomaterials can mitigate the agglomeration of graphene, and the substrate of graphene can also serve as barrier against the agglomeration of the nanomaterials anchored [9,10]. As a result, graphene nanohybrids are expected to achieve a better dispersion state than graphene alone in polymer matrices, if strong interactions are formed between them. The immobilization of foreign nanomaterials, such as magnetite nanoparticles and carbon nanotubes, on graphene nanosheets has been demonstrated to be an effective strategy for improving its dispersion [5,11]. In the graphene nanohybrids with other two-dimensional (2D) nanomaterials, larger contact area within hybrids is created in comparison to those of the nanohybrids containing zero-dimensional nanoparticles or one-dimensional nanowires. Graphene nanohybrids containing 2D nanomaterials display good dispersion in polymers. In a prior publication, we reported that the AlOOH nanoplatelets decorated on the graphene nanosheets can improve the dispersion of these two components [12].

For the non-charring PP, formation of carbonaceous protection layers on polymer surfaces during combustion plays a key role in the enhancement of flame retardancy. Transition metal compounds, such as nickel and cobalt, can efficiently catalyze carbonization of the degradation products of polyolefin, resulting in the reduced evolution of flammable pyrolysis gases and the improved flame retardancy [13].

Due to the combination of characteristics of 2D nanosheets and carbon nanomaterials, many efforts have been made to study the effects of graphene on the combustion behavior of various polymers [14–18]. Actually, incorporating graphene alone into polymers, such as PP, fails to obtain excellent flame retardancy [19]. This is mainly due to the poor dispersion and relatively low flame retardant efficiency of graphene. Thus, surface modification of graphene is particularly critical to enhance its flame retardant efficiency. Phosphorus or nitrogen containing flame retardants have been used to modify graphene (oxide). Cai et al. prepared a phosphazene flame retardant to simultaneously exfoliate and functionalize graphene, and then the functionalized graphene was applied to improve fire safety and mechanical properties of polyurethane [20]. Macromolecular flame retardants have been grafted onto graphene surface by "grafting to" or "grafting from" approaches. For example, Wang et al. covalently grafted polyphosphamide onto graphene nanosheets to enhance fire resistance of epoxy resin [21]. Furthermore, stronger interfacial compatibility between graphene and polymer is favorable for improving thermal stability of the resultant composites. Taking the advantages of transition metal catalyst and graphene, their nanohybrids are prepared to achieve enhanced flame retardant efficiency of graphene [22,23]. However, their dispersions are still unsatisfactory [22]. This may be due to the relatively weak interfacial interactions between graphene and the exogenous nanoparticles.

In recent years, phosphorus and nitrogen-containing flame retardants have received much attention, due to their high flame retardant efficiency and non-halogen characteristic. Phosphazene materials are a class of high performance flame retardant, because of the synergistic effects between phosphorus and nitrogen [24]. In this work, to improve the dispersion and flame retardant efficiency of GO, it was modified with phosphazene flame retardant and Ni$(OH)_2$ nanosheets. Removal of oxygen functional groups in GO and grafting of flame retardant are achieved synchronously. The NH_2 groups in this phosphazene flame retardant show strong affinity with Ni^{2+} and thus the decoration of Ni$(OH)_2$ nanosheets on the graphene is facilitated. The effect of functionalized graphene oxide (FGO) on the combustion property of PP is investigated and the enhancement mechanism is clearly demonstrated.

2. Experimental

2.1. Materials

Graphite powder (granularity $\leq$ 30 μm), triethylamine (TEA), p-phenylenediamine (PPD), tetrahydrofuran (THF), nickel chloride hexahydrate ($NiCl_2{\cdot}6H_2O$), ammonium hydroxide (25–28%), xylene and ethanol were purchased from Sinopharm Chemical Reagent Co., Ltd. TEA and THF were dried by 4 Å molecular sieves before being used. Hexachlorocyclotriphosphazene (HCCP) was kindly provided by Zibo Lanyin Chemical Co., Ltd. Isotactic PP homopolymer with a melt flow index (MFI) of 2.2 g/10 min (230 °C, 2.16 kg, ISO 1133) was supplied by Sinopec Yangzi Petrochemical Co., Ltd. Maleic anhydride grafted polypropylene (MAPP) (a MFI of 51.0 g/10 min, 0.8 wt% of maleic anhydride) was obtained from Suzhou Enhand New Materials Co., Ltd.

2.2. Preparation of dually-modified GO with phosphazene flame retardant and Ni$(OH)_2$ nanosheets

Graphite oxide was prepared by a modified Hummers method using graphite powder as raw material [25]. 3 g of graphite oxide was dispersed in 600 mL of THF with the assistance of continual mechanical stirring and ultrasonication for 30 min. 7.04 g of TEA was added to the GO dispersion in a 1000 mL round-bottom flask, and then HCCP solution comprising of 12 g HCCP and 50 mL THF was added dropwise to the mixture. The reaction was conducted at 50 °C for 12 h under N_2 protection. Then, 14.08 g of TEA and 22.36 g of PPD in 100 mL of THF were slowly added to the mixture. Afterwards, the reaction was maintained at 50 °C for 12 h. Next, the mixture was further treated by adding 4 g of deionized water and was maintained for 3 h. The resultant product was separated by filtration and rinsing copiously with THF and water, and then dried in a hot air oven at 80 °C. This product was designated as FGO1.

2 g of FGO1 and 20 g of $NiCl_2{\cdot}6H_2O$ was dispersed in 600 mL of water by stirring and ultrasonication for 30 min. 5 wt% ammonium hydroxide aqueous solution was added dropwise to the mixture with vigorous mechanical stirring until the pH value reached 9.5. The reaction was allowed to continue for 3 h. This product (FGO2) was extracted from the solution by filtration and washed thoroughly with water until the filtrate became colorless and neutral. The product obtained was dried at 100 °C for 12 h.

2.3. Fabrication of PP composites

PP composites comprising 2 wt% nanofillers (GO or FGO) were prepared by master batch-based melt mixing method, which was described in our prior publication [19]. Firstly, nanofiller/MAPP master batch was prepared by solution blending. Then, the master batch was melt mixed with the resin to prepare PP composites. The sheets for characterization were prepared by compression molding the melt-mixed samples in a press vulcanizer.

2.4. Characterization

Fourier transform infrared (FTIR) study was performed on a Nicolet 6700 spectrophotometer in the wavenumber range of 4000–400 cm^{-1}. Crystal structure of samples was characterized by a Rigaku TTR-III X-ray diffractometer (XRD) with Cu Kα radiation (λ = 0.1542 nm). Thermal stability of nanomaterials and its composites was investigated on a TA Q5000IR thermo-analyzer

at a heating rate of 20 °C/min. X-ray photoelectron spectroscopy (XPS) measurement was performed using a Thermo VG ESCALAB 250 electron spectrometer with an Al Kα line as the X-ray source (1486.6 eV). Transmission electron microscopy (TEM) was used to investigate the morphology of nanomaterials and their dispersion states in the matrix. The nanomaterials were dispersed in ethanol by ultrasonication and then dripped onto copper TEM grids. Composite film was microtomed into 20–100 nm thick ultrathin slices using a Cambridge ultratome and then transferred onto copper grids. Micrographs were obtained using a JEOL JEM-2100F microscope with an acceleration voltage of 200 kV. Composite film was immersed in liquid nitrogen and then fractured. The fractured surface was analyzed using a FEI Sirion 200 scanning electron microscope (SEM) at an acceleration voltage of 5 kV. The evolved gaseous decomposition products were studied by thermogravimetric analysis-infrared spectrometry (TG-IR), using a PerkinElmer TGA analyzer coupled with a Fourier transform infrared spectrophotometer. The testing was under helium flow and the heating rate was 20 °C/min. A FTT cone calorimeter was employed to investigate the combustion behavior. The sample with the size of $100 \times 100 \times 3$ mm^3 was wrapped in an aluminum foil and burned under 35 kW/m^2 external heat flux according to ISO 5660. Raman spectrum of char was taken with a LABRAM-HR laser confocal microRaman spectrometer equipped with a 514.5 nm laser source.

3. Results and discussion

3.1. Preparation procedure

A three-step strategy is employed to decorate flame retardant and nanomaterials on GO nanosheets. HCCP is firstly immobilized on GO nanosheets via the reactions between P—Cl and hydroxyl groups in GO. The second step is the grafting procedure via the in-situ polycondensation of HCCP and PPD under the catalysis of TEA. Finally, the $Ni(OH)_2$ nanosheets are nucleated and grew on the amine-capped FGO1. The preparation procedure is illustrated in Fig. 1.

3.2. Characterization of FGO

Functional groups in the products obtained are investigated with FTIR. The spectra of GO, FGO1 and FGO2 are shown in Fig. 2a. GO shows the characteristic C=O, C—O—C and C—OH groups at approximately 1730, 1220 and 1048 cm^{-1} [26,27], respectively. The peaks at around 1270, 1184 and 827 cm^{-1} in the spectrum of FGO1 are attributed to the phosphazene ring [28]. The absorption peak of P—NH—Ph appears at 935 cm^{-1} [29]. The bands at 1510 and 1380 cm^{-1} are ascribed to N—H bending and C—N stretching vibrations [29,30], respectively. The decrease in the intensity of oxygen functional groups for FGO1 is an indicative of the reduction of GO during the preparation reaction. In the FTIR spectrum of FGO2, an additional peak at 634 cm^{-1} is attributed to Ni—O vibration [31]. No characteristic absorption for P—Cl is observed at 606 and 523 cm^{-1} in the spectra of FGO1 and FGO2, suggesting the complete substitution reaction of P—Cl in HCCP by PPD.

XRD pattern of GO shows a sharp peak at 10.7°, corresponding to an interlayer spacing of 0.827 nm (Fig. 2b). This strong diffraction peak in FGO1 shifts to 8.7°. This enlarged interlayer spacing of FGO1 indicates that the flame retardant has been intercalated into the interlayer region of GO. There is no obvious diffraction peak of the phosphazene flame retardant, implying its amorphous structure. The broad peak at around 21° is attributed to disordered graphitic platelets, indicating the chemical reduction of GO under the alkaline environment [32,33].

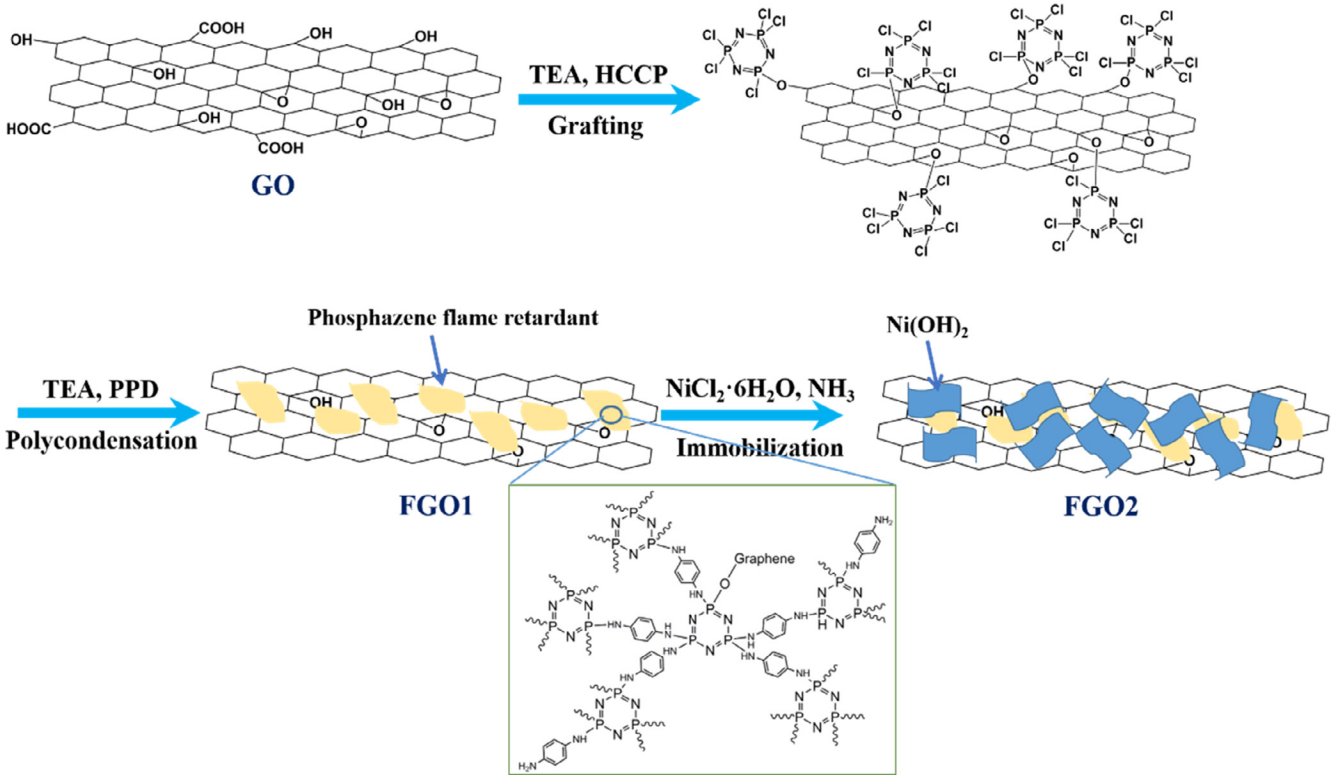

Fig. 1. The preparation route of FGO. (For interpretation of the references to colour in this figure legend, the reader is referred to the web version of this article.)

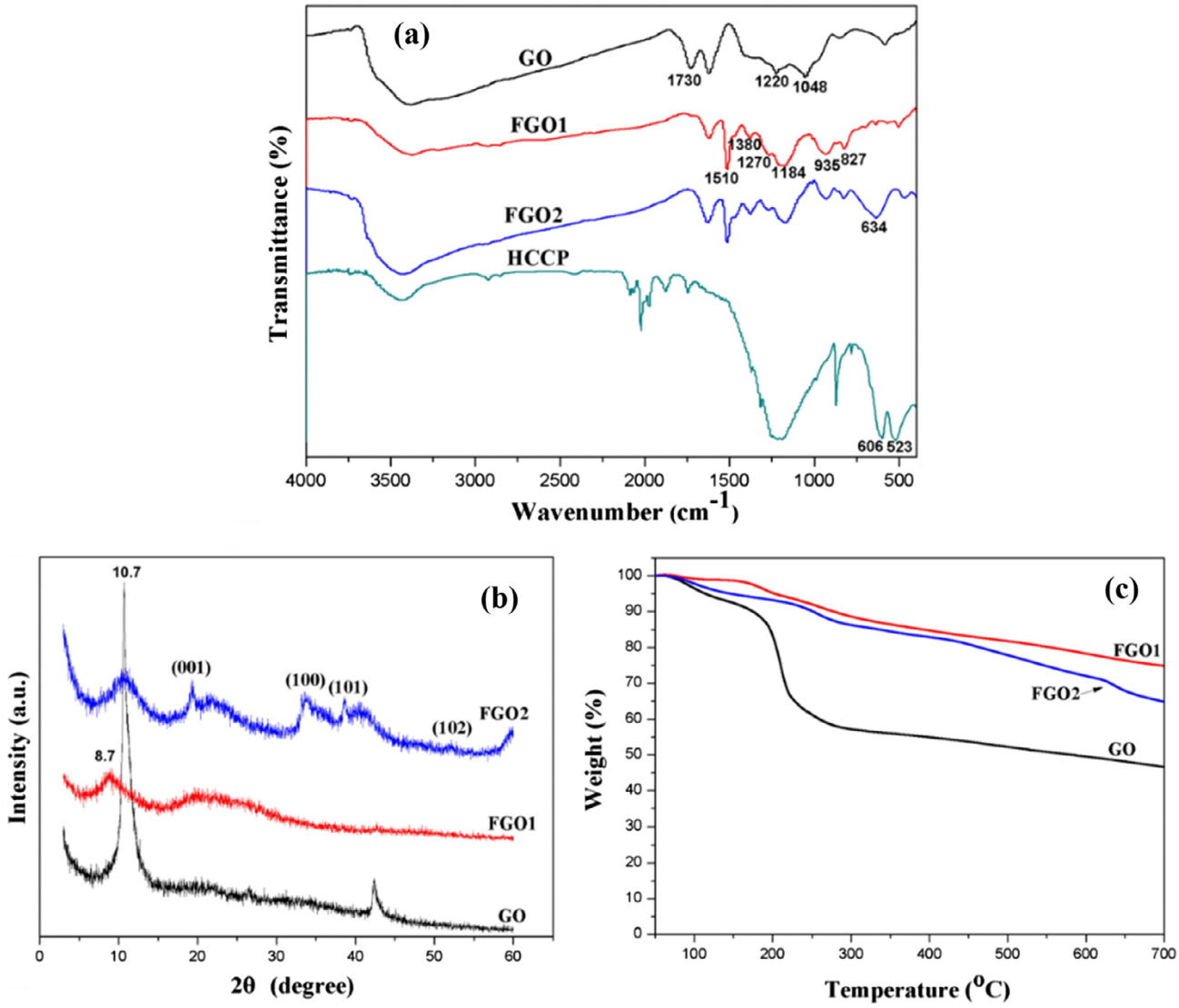

Fig. 2. (a) FTIR spectra, (b) XRD patterns and (c) TGA curves of GO and FGO. (For interpretation of the references to colour in this figure legend, the reader is referred to the web version of this article.)

XRD pattern of FGO2 shows the characteristic peaks of $Ni(OH)_2$ at 19.4, 33.5, 38.6 and 51.7°, corresponding to (001), (100), (101) and (102) crystal planes (JCPDS 14-0117) [34], respectively.

As shown in Fig. 2c, GO is a thermally unstable material with two main weight loss stages at around 90 and 210 °C, corresponding to the removal of moisture and labile oxygen functional groups [26], respectively. After functionalization, its thermal stability is greatly enhanced. The gradual weight loss above 300 °C in the TGA curve of FGO1 is assigned to thermal decomposition of phosphazene flame retardant. The marked weight loss stage between 175 and 315 °C in the TGA curve of FGO2 is mainly due to the dehydration decomposition of $Ni(OH)_2$. The residual weights for FGO1 and FGO2 at 700 °C are determined to be 74.9 wt% and 64.9 wt%, respectively, which are greater than that of GO.

XPS is used to detect the chemical composition of GO and FGO. XPS spectra are shown in Fig. 3 and the data on chemical composition are provided in Table 1. The survey XPS spectrum of FGO1 shows C, N and P elements, and no Cl peaks is observed (Fig. 3a), indicating the flame retardant has been successfully synthesized and the Cl atoms in HCCP have been completely substituted by PPD. To further present the evidence of successful preparation of FGO, high-resolution XPS spectra are shown in Fig. 3b–e. C 1s spectrum of GO (Fig. 3b) shows typical peaks: sp^2 carbon components (284.8 eV), hydroxyl groups (286.7 eV), epoxy groups (287.3 eV) and carbonyl functionalities (288.3 eV) [35–38]. C 1s spectrum of FGO1 indicates the presence of C—O—P/C—N groups (285.3 eV) (Fig. 3c) [39]. Furthermore, the intensity of oxygen functional groups in FGO1 decreases, suggesting the reduction functions of the alkaline environment and PPD. The deconvoluted N 1s XPS spectrum of FGO1 is associated with four bands: P═N (397.6 eV), P—NH—Ph (399.0 eV), Ph—NH_2 (399.7 eV) and protonated nitrogen (400.9 eV) [29] (Fig. 3d). These results suggest that the phosphazene flame retardant with free NH_2 groups has been grafted on the surface of GO nanosheets. These NH_2 groups will greatly improve the affinity of graphene with Ni^{2+}, which will form strong interfacial interactions. In the XPS spectrum of FGO2, the peaks corresponding to Ni are observed. Ni 2p XPS spectrum in Fig. 3d shows two major peaks centered at 875.1 eV (Ni 2p1/2) and 857.1 eV (Ni 2p3/2) with a spin-energy separation of 18.0 eV, which is an indicative of the formation of $Ni(OH)_2$ [31]. It should be noted that the related peaks of P and N are not marked in the spectrum of FGO2, because XPS is a surface detection technique

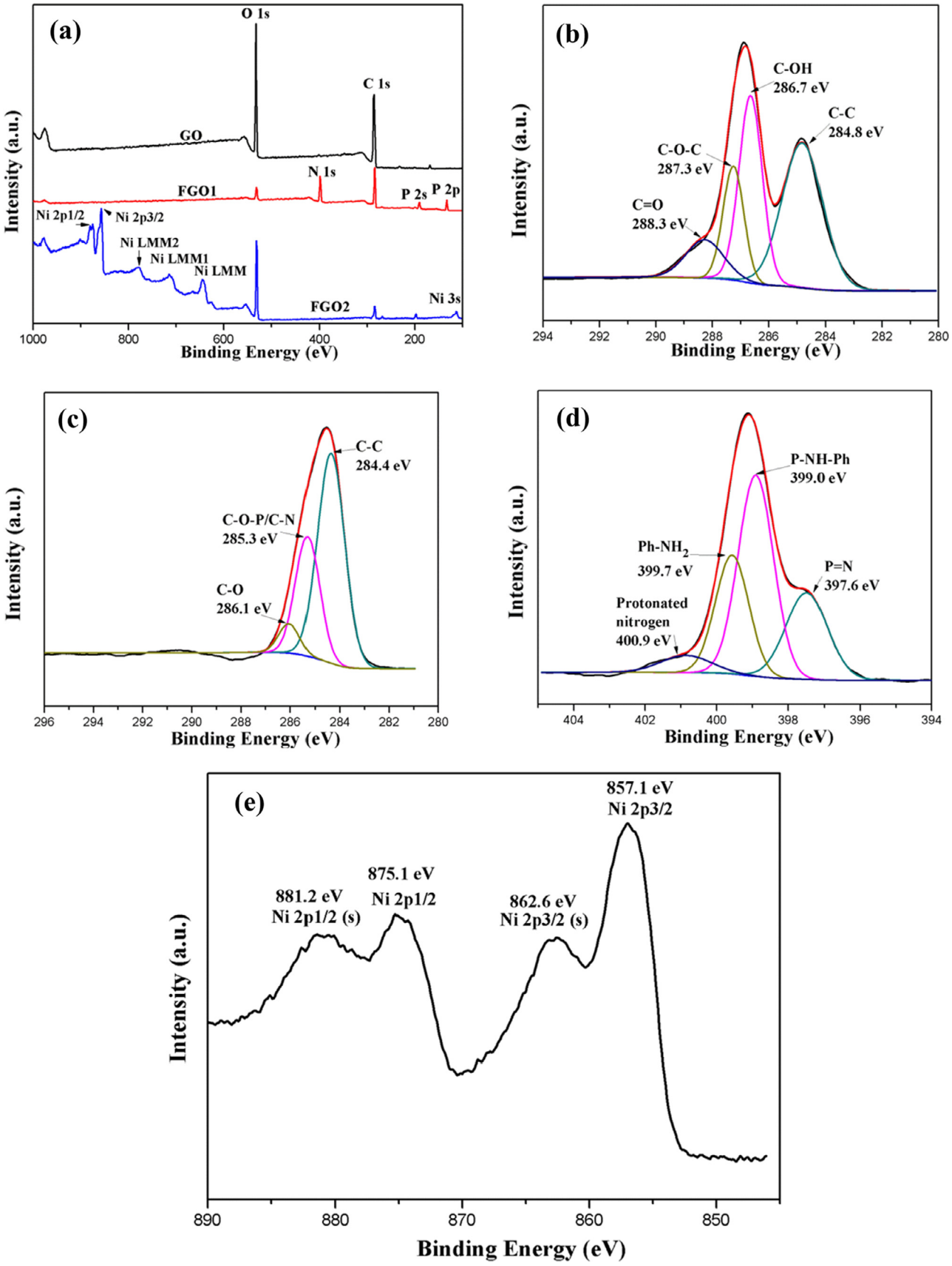

Fig. 3. (a) XPS survey spectra of GO and FGO; (b) C 1s spectrum of GO; (c) C 1s and (d) N 1s spectra of FGO1; (e) Ni 2p spectrum of FGO2. (For interpretation of the references to colour in this figure legend, the reader is referred to the web version of this article.)

Table 1
Element content of GO, FGO1 and FGO2 measured from XPS analysis.

Sample	C (at.%)	O (at.%)	P (at.%)	N (at.%)	Ni (at.%)
GO	61.61	38.39	–	–	–
FGO1	56.23	9.43	7.82	26.52	–
FGO2	19.71	49.99	0.45	1.13	28.72

and the underlying flame retardants are shielded by the $Ni(OH)_2$ nanosheets. Furthermore, the signals of flame retardants are visible in the FTIR spectrum of FGO2. Due to the strong electrostatic interactions between NH_2 groups in the phosphazene and $Ni(OH)_2$, the N 1s peak for FGO2 is downshifted and broadened (Fig. S1, Supplementary material) [19,40]. These results provide solid evidences for successful functionalization of GO with phosphazene flame retardant and $Ni(OH)_2$.

Morphology of the graphene-based products is revealed by TEM, as shown in Fig. 4. TEM image of GO shows the appearance of electron beam transparency and wrinkle. TEM image of FGO1 reveals that flame retardants with nanosheet structure are grafted on the GO nanosheets, indicating that the GO acts as a template for the preparation of phosphazene flame retardant. EDX is used to

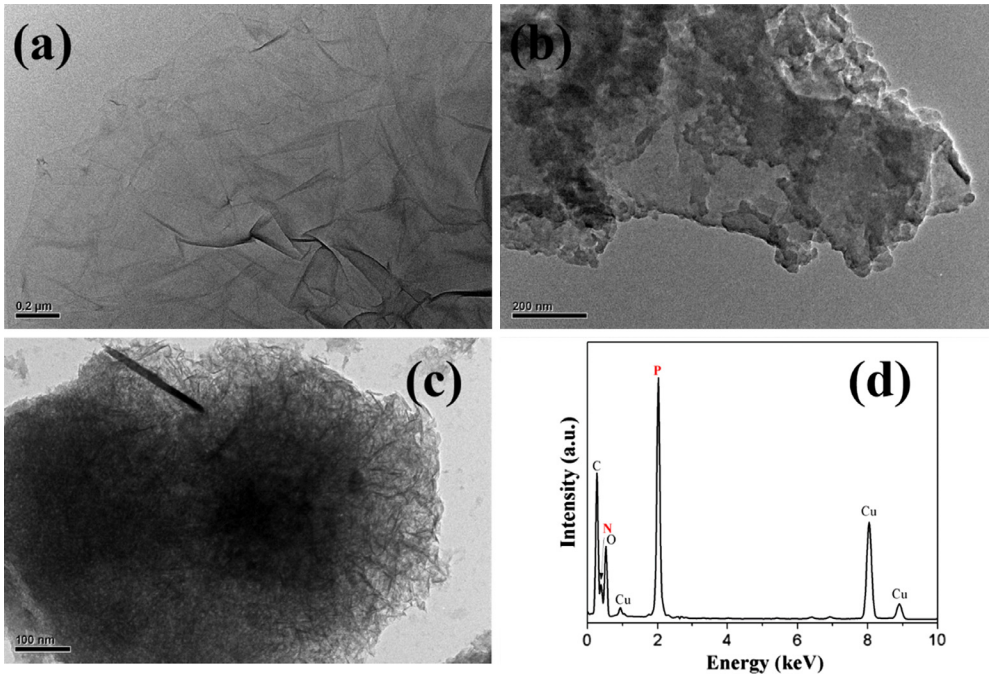

Fig. 4. TEM images of (a) GO, (b) FGO1 and (c) FGO2; (d) EDX spectrum of FGO1. (For interpretation of the references to colour in this figure legend, the reader is referred to the web version of this article.)

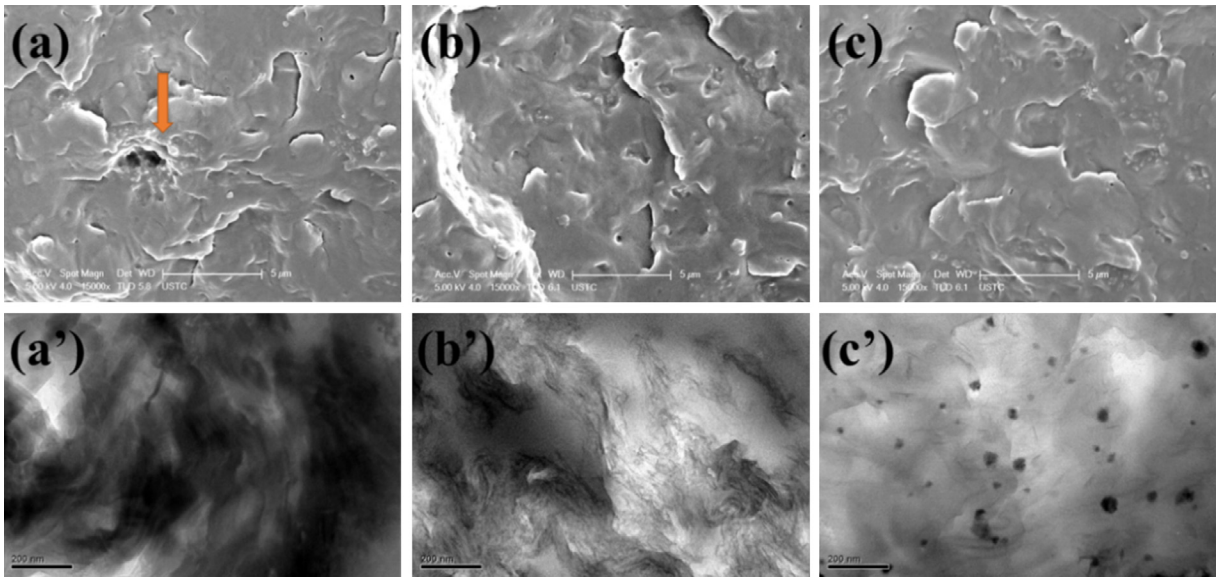

Fig. 5. SEM micrographs of the freeze-fractured surface of (a) GO/PP, (b) FGO1/PP and (c) FGO2/PP; TEM images of the ultrathin slices of (a′) GO/PP, (b′) FGO1/PP and (c′) FGO2/PP. (For interpretation of the references to colour in this figure legend, the reader is referred to the web version of this article.)

track the surface element in FGO1. The presence of N and P on FGO1 nanosheet is confirmed by these signals in the EDX spectrum. From TEM image of FGO2, it is apparent that graphene nanosheets are densely coated with $Ni(OH)_2$ nanosheets. Because of strong interactions, the immobilization of $Ni(OH)_2$ on FGO1 nanosheets is promoted. These decorated nanosheets can inhibit the agglomeration and restacking of graphene, thus the dispersion of graphene in PP matrix is logically expected to be enhanced.

3.3. Dispersion of FGO in the PP matrix

Dispersion of GO and FGO in the matrix is characterized with SEM and TEM. SEM images provide the information of graphene dispersion on micrometer scale. Large GO agglomerates are observed in the SEM image of GO/PP composite, as indicated by an arrow (Fig. 5a). However, the FGO shows better dispersion in the PP matrix without marked stacking graphene nanosheets (Fig. 5b and c). Dispersion state of GO and FGO in the matrix is further investigated with TEM (Fig. 5a′–c′). It is apparent that the GO is dispersed in the matrix as the form of aggregates. TEM images with higher magnification for FGO1/PP and FGO2/PP are shown in Figs. S2 and S3, respectively (Supplementary material). Generally, the FGO1 nanosheets are evenly distributed in the matrix, although some restacking nanosheets are observed. Undoubtedly, the dispersion of FGO1 is markedly enhanced, owing to the organic modification. Via functionalization, the compatibility between graphene and polymer is improved, resulting in better dispersion. In TEM image of FGO2/PP, the nanomaterials with homogeneous dispersion are unambiguously observed. This may be explained by the fact that the synergetic dispersion effect of FGO1 and $Ni(OH)_2$ nanosheets leads to the improved dispersion. The dispersion or agglomeration of nanofillers within polymer matrix also depends on their length [41]. From the TEM image of FGO2/PP in Fig. S3, it can be observed that the length of graphene is in the range of 50–250 nm.

3.4. Thermal stability and thermal decomposition

Thermal decomposition behavior of PP and its composites is investigated with TGA. TGA and differential thermogravimetric (DTG) curves are presented in Fig. 6 and the detailed data are summarized in Table 2. $T_{initial}$ is defined as the temperature at which the weight loss is 5 wt%. PP and its composites exhibit one-step thermal decomposition under nitrogen and air atmosphere, corresponding to thermal degradation of polymer backbone. From the TGA curves in nitrogen, it can be seen that thermal stability of PP composites is similar to that of neat PP. Furthermore, residual weights of FGO/PP composites are greater than those of neat PP and GO/PP. Under air atmosphere, compared with neat PP, GO/PP shows poorer stability, due to the thermally unstable feature of GO. However, thermal stability of FGO1/PP is greatly enhanced. For example, T_{max} of FGO1/PP is 17 °C higher than that of neat

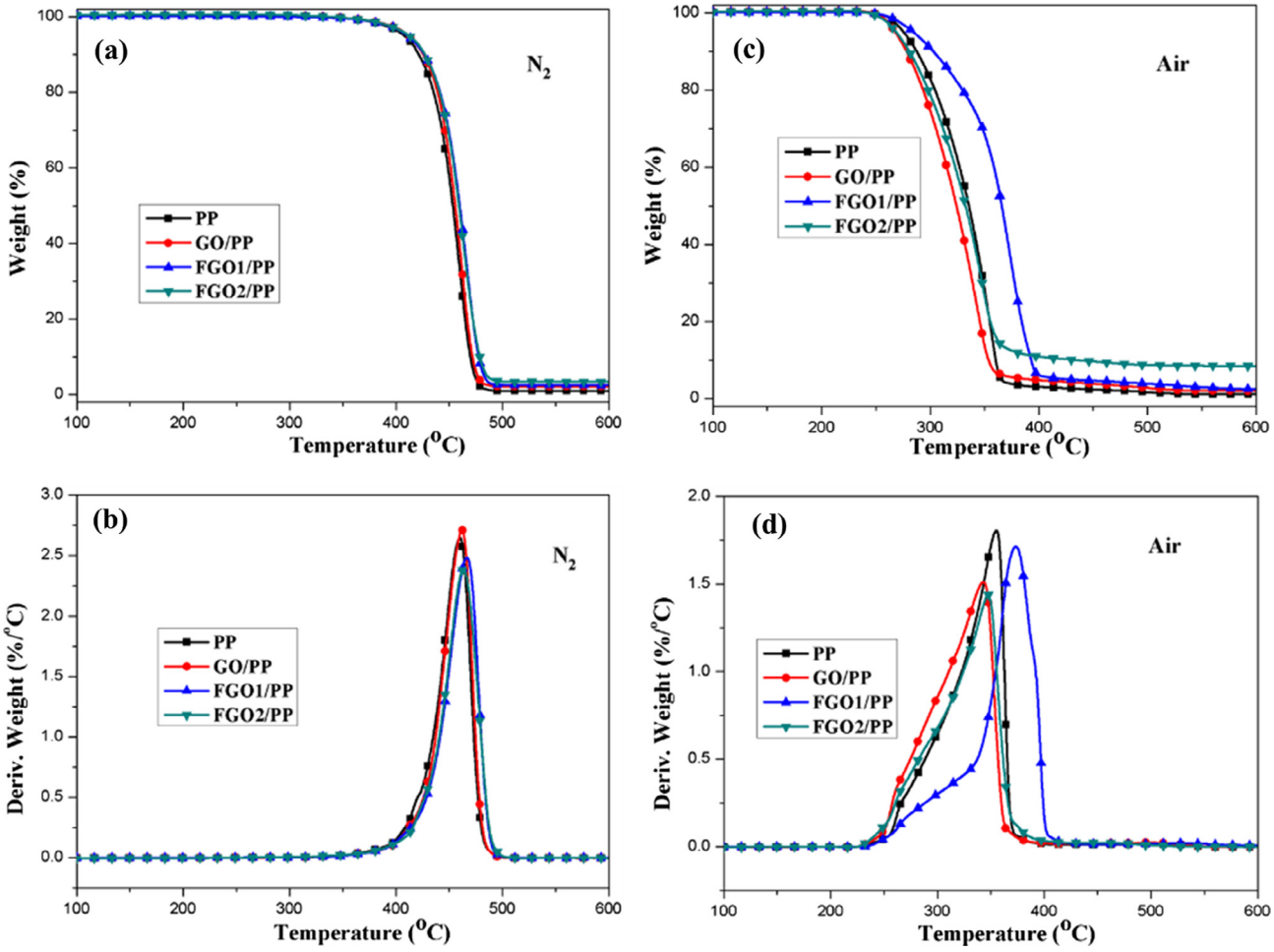

Fig. 6. TGA and DTG curves of PP and its composites under (a, b) N_2 and (c, d) air atmosphere. (For interpretation of the references to colour in this figure legend, the reader is referred to the web version of this article.)

Table 2
TGA data of PP and its composites.

Sample	$T_{initial}$ (°C)		T_{max} (°C)		Char residue (wt%)	
	N_2	Air	N_2	Air	N_2	Air
PP	408	275	460	356	1.09	1.55
GO/PP	411	268	462	343	2.20	2.16
FGO1/PP	411	285	467	373	2.48	2.18
FGO2/PP	412	269	463	348	3.62	8.56

PP. The strong interfacial interactions between nanofillers and polymer matrix can increase thermal degradation activation energy of the composites via restriction thermal motion of polymer chains [42,43]. The catalytic charring effect of FGO2 is responsible for the decreased thermal stability and increased char yield of its nanocomposite [13]. Impressively, the incorporation of 2 wt% FGO2 into PP increases residual char from 1.55 to 8.56 wt%. That is, the modification with flame retardant and $Ni(OH)_2$ enhances the charring function of GO. The increased char yield of the composites signifies that part of polymer matrix cannot be completely combusted, leading to enhanced flame retardancy. From DTG curves, it is apparent that maximum mass loss rates of the composites are decreased by FGO, because of the physical barrier effect of well-dispersed FGO on the emission of volatile degradation products.

To investigate the influence of FGO on the evolved volatiles during pyrolysis, the volatile components released from PP and its composites are monitored by TG-IR, as shown in Fig. 7. FTIR absorption spectrum of pyrolysis products of the samples at the maximum decomposition rate is presented in Fig. 7a. Main gaseous products are saturated hydrocarbons (2964, 2930, 1458 and 1380 cm^{-1}), unsaturated alkane (3080, 1645 and 890 cm^{-1}) and CO_2 (2362 cm^{-1}) [44]. The peaks at 2964 and 890 cm^{-1} are used to characterize the intensity of the released saturated hydrocarbons and unsaturated alkane, respectively. As shown in Fig. 7b–d, the addition of FGO into PP matrix decreases the intensity of total

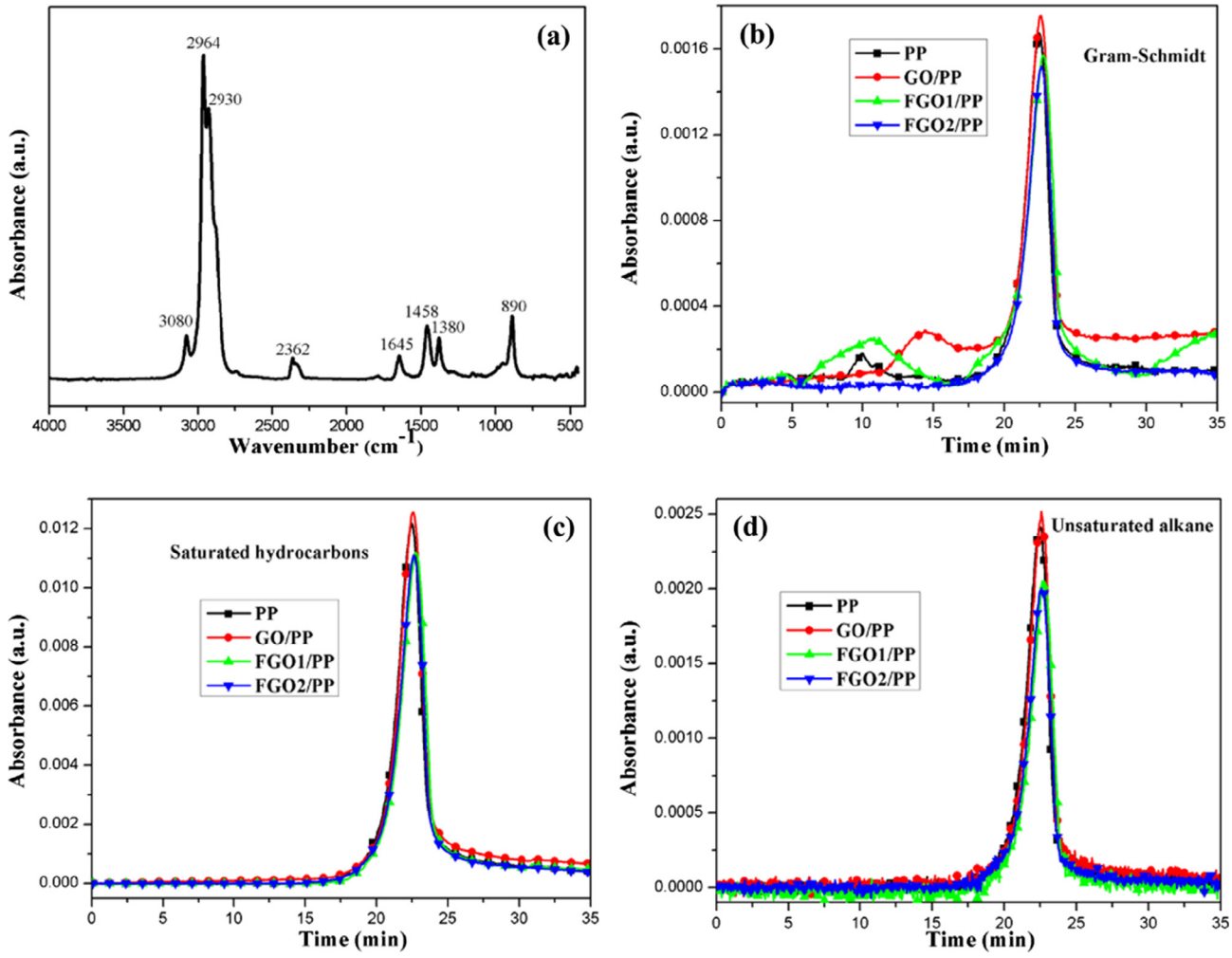

Fig. 7. (a) FTIR spectrum of the evolved pyrolysis gases at maximum mass loss rate; Absorbance curves of (b) total decomposition products, (c) saturated hydrocarbons and (d) unsaturated alkane versus time. (For interpretation of the references to colour in this figure legend, the reader is referred to the web version of this article.)

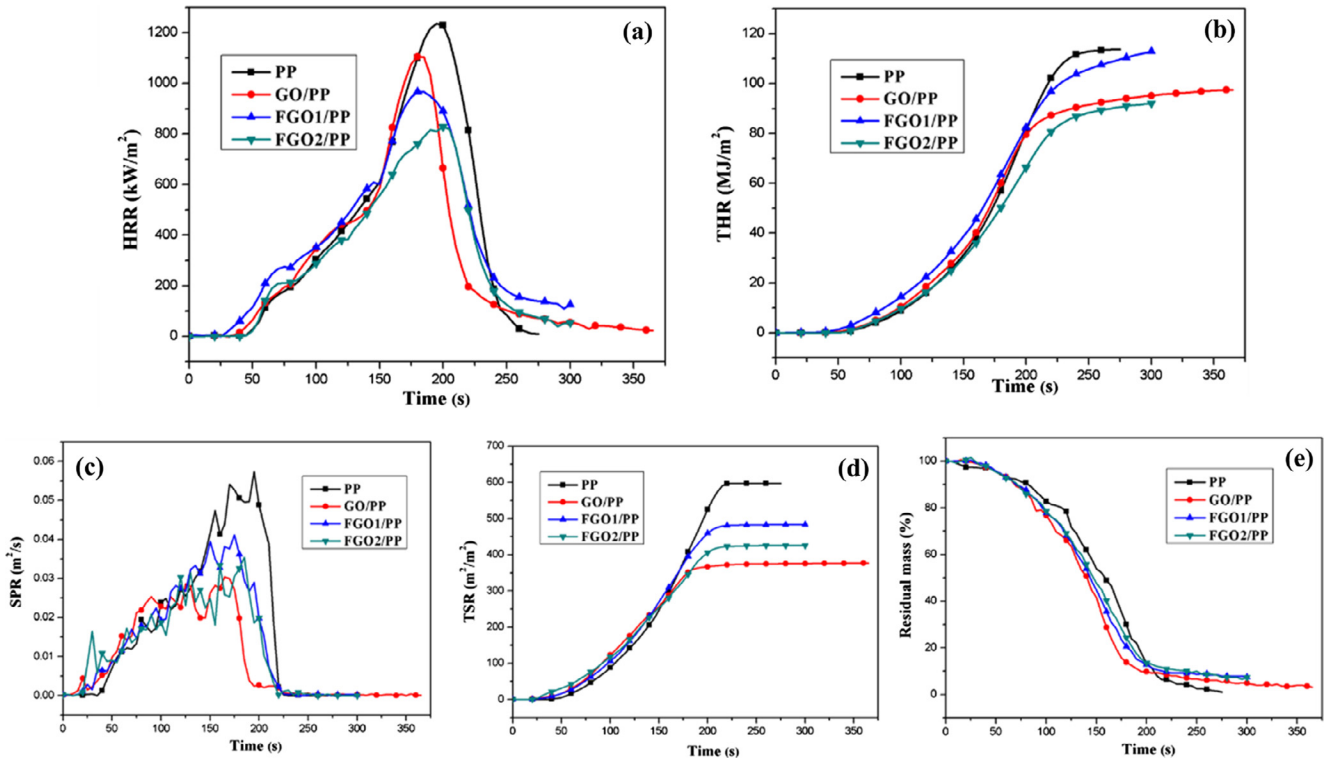

Fig. 8. (a) HRR, (b) THR, (c) SPR, (d) TSR and (e) normalized mass loss curves of PP and its composites. (For interpretation of the references to colour in this figure legend, the reader is referred to the web version of this article.)

Table 3
Cone calorimetry combustion data of PP and its composites.

Sample	TTI (s)	T_{PHRR} (s)	PHRR (kW/m^2)	THR (MJ/m^2)	Residue (wt%)	TSR (m^2/m^2)	FGI (kW/m^2 s)
PP	45	200	1230	113.6	0.97	597	6.15
GO/PP	30	180	1105	97.5	3.14	377	6.14
FGO1/PP	27	185	967	112.9	7.49	484	5.23
FGO2/PP	35	200	829	92.0	7.33	426	4.15

pyrolysis products, saturated hydrocarbons and unsaturated alkane, confirming the good barrier performance of FGO. However, the GO slightly increases the yield of flammable volatile degradation products. That is, the well-dispersed FGO can decrease the release rate of flammable pyrolysis products of PP. Furthermore, the $Ni(OH)_2$ nanosheets in FGO2 are expected to catalyze the pyrolysis products to form char, resulting in the reduction in release rate.

3.5. Combustion behavior

Cone calorimeter is a widely employed tool to characterize combustion behavior of polymers under forced fire scenario. Some important data, such as peak heat release rate (PHRR), total heat release (THR), time to ignition (TTI) and total smoke release (TSR), are exported from cone calorimeter to evaluate flame retardancy of PP and its composites. Heat and smoke release curves from cone calorimetry are shown in Fig. 8 and the related data are summarized in Table 3. TTI values of the composites are lower than that of neat sample, due to the enhanced heat absorption within the composites surface layer by graphene [44]. PHRR is the most important parameter to investigate combustion behavior of polymers. From HRR curves and Table 3, it can be seen that a decrease in PHRR is achieved in FGO1/PP and FGO2/PP (Fig. 8a). For example, compared with neat PP, the incorporation of FGO1 and FGO2 results in 21.4% and 32.6% reduction in PHRR, respectively. However, the PHRR value of GO/PP is just slightly lower than that of neat PP. Except for FGO1/PP, THR values of PP composites are greatly lower than that of neat PP (Fig. 8b). 19.0% reduction in THR is achieved in FGO2/PP, suggesting that part of PP matrix in the nanocomposite has been shielded from complete combustion. Ni nanomaterials can catalyze the decomposition products of PP to form stable char, resulting in the decrease in combustion fuel supply. Fire growth index (FGI), which is derived from the proportion of PHRR to time to PHRR (T_{PHRR}), is an important parameter to assess fire hazard of polymer materials [45]. As shown in Table 3, the FGI values of FGO1/PP and FGO2/PP are lower than those of neat PP and GO/PP, indicating higher fire safety for PP composites, especially for FGO2/PP. Smoke production rate (SPR) and TSR curves of neat PP and its composites are shown in Fig. 8c and d, respectively. Both SPR and TSR are decreased by the addition of GO or FGO. TSR value of FGO2/PP is drastically reduced from 597 m^2/m^2 for neat PP to 426 m^2/m^2, which corresponds to 28.6% reduction. Fig. 8e shows the curves of residual mass versus combustion time. The char yield obtained from Fig. 8e is displayed in Table 3. Residual mass of FGO1/PP and FGO2/PP are higher than

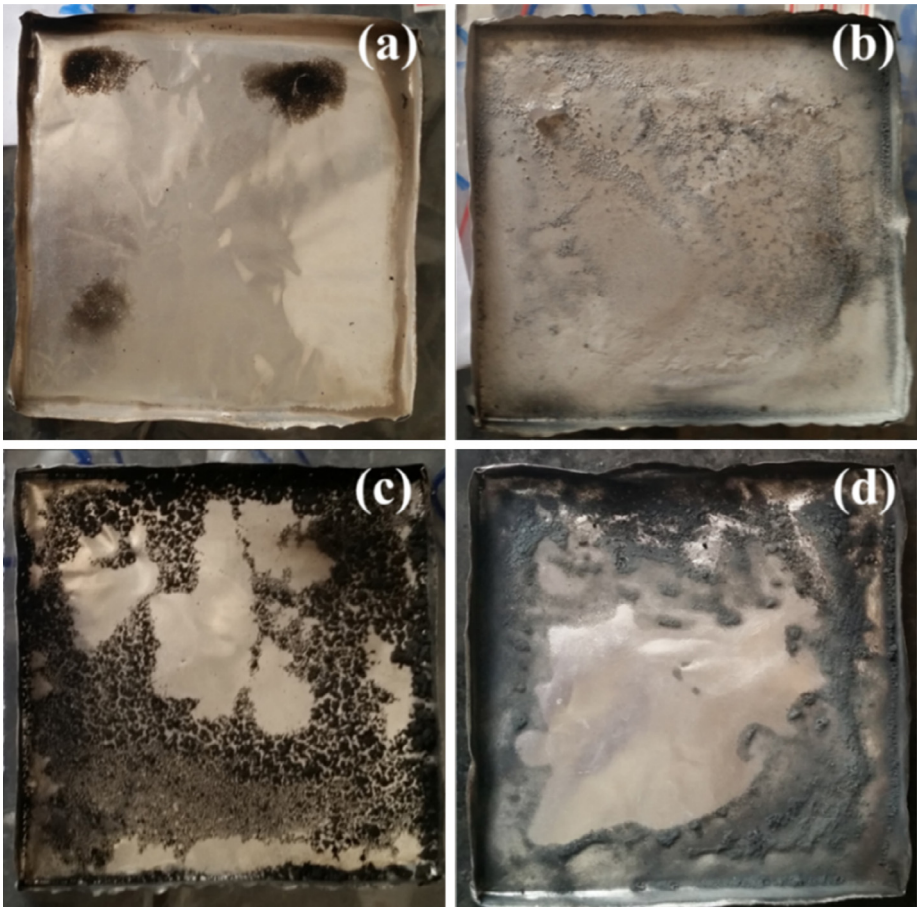

Fig. 9. Digital photos of the residual char of (a) PP, (b) GO/PP, (c) FGO1/PP and (d) FGO2/PP. (For interpretation of the references to colour in this figure legend, the reader is referred to the web version of this article.)

those of neat sample and GO composite. This means that more PP matrix has been shielded from complete combustion in the case of FGO/PP composites. The photographs of char residues of PP and its composites are presented in Fig. 9. There is almost no char left in the aluminum foil after the combustion of neat PP. In GO/PP, a few white particles remain, which are the combustion debris of GO. For FGO1/PP, the aluminum foil is covered by black solid product. Green and black solid is left after the cone calorimeter combustion of FGO2/PP, indicating the presence of graphene and Ni-based products in the char. As clearly shown in the discussion above, a conclusion can be drawn that GO-based nanomaterials, especially for FGO2, can greatly reduce fire risk of PP.

Raman spectroscopy is used to determine graphitization degree of char residue. The char with higher graphitization degree often possesses higher thermal oxidation resistance, which is beneficial in improving flame retardancy of polymer [46]. Raman spectra of the char are presented in Fig. 10a–c. Curve fitting of Raman data are conducted by using Origin 8.0 software with Lorentz mode. Generally, the integrated intensity ratio of D to G bands (I_D/I_G) is an indicative of graphitization degree of carbonaceous materials. Higher value of I_D/I_G indicates the lower graphitization degree. As shown in Fig. 10, I_D/I_G of GO/PP char residue (3.23) is higher than those of PP nanocomposites containing FGO1 (2.51) and FGO2 (2.59). The grafted flame retardant and anchored $Ni(OH)_2$ nanosheets can protect the GO nanosheets from serious damage, resulting in higher thermal stability of the combusted FGO. Fig. 10d shows the FTIR spectra of residual char, which provide information concerning chemical structure of residues. The peaks at around 1628 cm^{-1} and 1581 cm^{-1} are from the absorption of moisture and/or the characteristic peak of graphene [26]. The presence of 1108 cm^{-1} peak for C—O bonds confirms the oxidation of graphene under the combustion in cone calorimeter test. Two characteristic bands at 2957 and 2924 cm^{-1} in the spectra of FGO composites are attributed to the organic moieties in the char [28]. The absorption peaks at 1449 and 1444 cm^{-1} are due to the C—C stretching vibration of the carbonized products for phosphazene flame retardant [28]. The stretching vibrations of P—O—P bond are reflected by the peaks at 1090 and 950 cm^{-1} [47]. The absorption peaks of P═O and P—O—Ph appear at 1292 and 758 cm^{-1} [48,49], respectively, in the spectrum of FGO1/PP char. The strong peak at 497 cm^{-1} is also from the phosphorus-containing materials (O—P—O) [50]. As shown in FTIR spectra, the residual materials in the char for FGO2/PP are similar to those of FGO1/PP. It can be deduced from these spectra that the residual char of FGO/PP is composed of graphite materials and cross-linked phosphorus-containing compounds, which can provide an effective barrier against mass and heat diffusion.

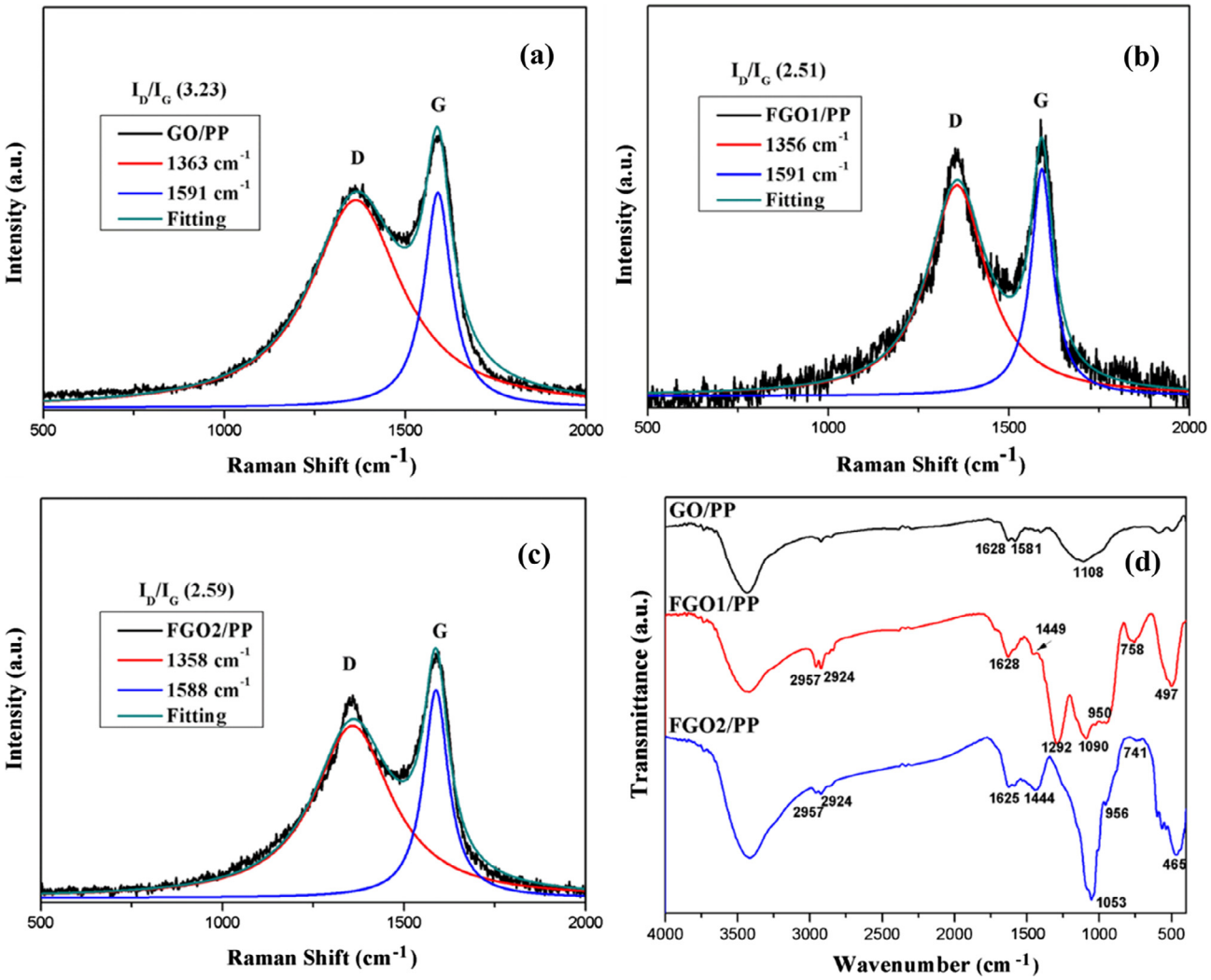

Fig. 10. Raman spectra of char residues of (a) GO/PP, (b) FGO1/PP, (c) FGO2/PP and (d) FTIR spectra of the char residues. (For interpretation of the references to colour in this figure legend, the reader is referred to the web version of this article.)

4. Conclusions

In this work, a novel method to improving dispersion and flame retardant efficiency of GO/graphene was proposed. GO was dually modified with polymeric flame retardant and the nanomaterial with catalytic carbonation ability. Phosphazene flame retardant was grafted on GO nanosheets and then $Ni(OH)_2$ nanosheets were loaded on the surface of the amine-rich FGO1 nanosheets via the strong interactions between NH_2 groups and Ni^{2+}. The reduction of GO was achieved during the preparation. GO nanosheets served as the template for grafting of flame retardant and FGO1 nanosheets provided substrate for the loading of $Ni(OH)_2$. The modification enhanced thermal stability of GO and its dispersion in PP matrix. Relative to pristine GO, the covalent attachment of phosphazene flame retardant and immobilization of $Ni(OH)_2$ nanosheets effectively improved the dispersion of graphene in polymer matrix. The FGO increased the char yield of the composites and reduced the emission of flammable volatile products. PHRR, THR and smoke release of PP were decreased by FGO, especially for FGO2. The remarkable enhancement in fire safety was mainly attributed to the barrier effect of graphene nanosheets, flame retardant function of phosphazene modifier and catalytic charring performance of $Ni(OH)_2$.

Acknowledgements

This work was supported by the National Key Technologies Research and Development Program of China (grant number 2016YFC0802801), the Natural Science Foundation of China (grant numbers 51374164 and 21374111), the Fundamental Research Funds for the Central Universities (grant number WUT: 2017IVA043) and the Open Research Fund of State Key Laboratory of Coal Mine Safety Technology (grant number sklcmst103).

Appendix A. Supplementary material

Supplementary data associated with this article can be found, in the online version, at http://dx.doi.org/10.1016/j.compositesa.2017.04.012.

References

[1] Hu K, Kulkarni DD, Choi I, Tsukruk VV. Graphene-polymer nanocomposites for structural and functional applications. Prog Polym Sci 2014;39(11):1934–72.
[2] Layek RK, Nandi AK. A review on synthesis and properties of polymer functionalized graphene. Polymer 2013;54(19):5087–103.
[3] Hsiao MC, Liao SH, Yen MY, Liu PI, Pu NW, Wang CA, et al. Preparation of covalently functionalized graphene using residual oxygen-containing functional groups. ACS Appl Mater Interfaces 2010;2(11):3092–9.

[4] Fang M, Wang K, Lu H, Yang Y, Nutt S. Covalent polymer functionalization of graphene nanosheets and mechanical properties of composites. J Mater Chem 2009;19(38):7098–105.
[5] Yang S-Y, Lin W-N, Huang Y-L, Tien H-W, Wang J-Y, Ma C-CM, et al. Synergetic effects of graphene platelets and carbon nanotubes on the mechanical and thermal properties of epoxy composites. Carbon 2011;49(3):793–803.
[6] Singh AP, Mishra M, Chandra A, Dhawan SK. Graphene oxide/ferrofluid/cement composites for electromagnetic interference shielding application. Nanotechnology 2011;22(46):465701.
[7] Fang M, Chen Z, Wang S, Lu H. The deposition of iron and silver nanoparticles in graphene-polyelectrolyte brushes. Nanotechnology 2012;23(8):085704.
[8] Pei S, Cheng H-M. The reduction of graphene oxide. Carbon 2012;50(9):3210–28.
[9] Li XY, Huang XL, Liu DP, Wang X, Song SY, Zhou L, et al. Synthesis of 3D hierarchical Fe3O4/graphene composites with high lithium storage capacity and for controlled drug delivery. J Phys Chem C 2011;115(44):21567–73.
[10] Liu YW, Guan MX, Feng L, Deng SL, Bao JF, Xie SY, et al. Facile and straightforward synthesis of superparamagnetic reduced graphene oxide-Fe3O4 hybrid composite by a solvothermal reaction. Nanotechnology 2013;24(2):35.
[11] Liu P, Zhong W, Wu X, Qiu J. Facile synergetic dispersion approach for magnetic Fe3O4@graphene oxide/polystyrene tri-component nanocomposite via radical bulk polymerization. Chem Eng J 2013;219:10–8.
[12] Yuan BH, Bao CL, Qian XD, Jiang SH, Wen PY, Xing WY, et al. Synergetic dispersion effect of graphene nanohybrid on the thermal stability and mechanical properties of ethylene vinyl acetate copolymer nanocomposite. Ind Eng Chem Res 2014;53(3):1143–9.
[13] Wen X, Gong J, Yu HO, Liu Z, Wan D, Liu J, et al. Catalyzing carbonization of poly(L-lactide) by nanosized carbon black combined with Ni2O3 for improving flame retardancy. J Mater Chem 2012;22(37):19974–80.
[14] Shi Y, Yu B, Duan L, Gui Z, Wang B, Hu Y, et al. Graphitic carbon nitride/phosphorus-rich aluminum phosphinates hybrids as smoke suppressants and flame retardants for polystyrene. J Hazard Mater 2017;332:87–96.
[15] Xing W, Yang W, Yang W, Hu Q, Si J, Lu H, et al. Functionalized carbon nanotubes with phosphorus- and nitrogen-containing agents: effective reinforcer for thermal, mechanical, and flame-retardant properties of polystyrene nanocomposites. ACS Appl Mater Interfaces 2016;8(39):26266–74.
[16] Yang W, Jia Z, Chen Y, Zhang Y, Si J, Lu H, et al. Carbon nanotube reinforced polylactide/basalt fiber composites containing aluminium hypophosphite: thermal degradation, flame retardancy and mechanical properties. RSC Adv 2015;5(128):105869–79.
[17] Li X, Wang Z, Wu L. Preparation of a silica nanospheres/graphene oxide hybrid and its application in phenolic foams with improved mechanical strengths, friability and flame retardancy. RSC Adv 2015;5(121):99907–13.
[18] Chen X, Ma C, Jiao C. Synergistic effects between iron-graphene and ammonium polyphosphate in flame-retardant thermoplastic polyurethane. J Therm Anal Calorim 2016;126(2):633–42.
[19] Yuan BH, Song L, Liew KM, Hu Y. Solid acid-reduced graphene oxide nanohybrid for enhancing thermal stability, mechanical property and flame retardancy of polypropylene. RSC Adv 2015;5(51):41307–16.
[20] Cai W, Feng X, Wang B, Hu W, Yuan B, Hong N, et al. A novel strategy to simultaneously electrochemically prepare and functionalize graphene with a multifunctional flame retardant. Chem Eng J 2017;316:514–24.
[21] Wang X, Xing W, Feng X, Yu B, Song L, Hu Y. Functionalization of graphene with grafted polyphosphamide for flame retardant epoxy composites: synthesis, flammability and mechanism. Polym Chem 2014;5(4):1145–54.
[22] Bao C, Song L, Wilkie CA, Yuan B, Guo Y, Hu Y, et al. Graphite oxide, graphene, and metal-loaded graphene for fire safety applications of polystyrene. J Mater Chem 2012;22(32):16399–406.
[23] Wang D, Kan Y, Yu X, Liu J, Song L, Hu Y. In situ loading ultra-small Cu2O nanoparticles on 2D hierarchical TiO2-graphene oxide dual-nanosheets: Towards reducing fire hazards of unsaturated polyester resin. J Hazard Mater 2016;320:504–12.
[24] Tao K, Li J, Xu L, Zhao XL, Xue LX, Fan XY, et al. A novel phosphazene cyclomatrix network polymer: design, synthesis and application in flame retardant polylactide. Polym Degrad Stabil 2011;96(7):1248–54.
[25] Hummers WS, Offeman RE. Preparation of graphitic oxide. J Am Chem Soc 1958;80(6):1339.
[26] Yuan B, Bao C, Qian X, Song L, Tai Q, Liew KM, et al. Design of artificial nacre-like hybrid films as shielding to mitigate electromagnetic pollution. Carbon 2014;75:178–89.
[27] Gu J, Dong W, Xu S, Tang Y, Ye L, Kong J. Development of wave-transparent, light-weight composites combined with superior dielectric performance and desirable thermal stabilities. Compos Sci Technol 2017;144:185–92.
[28] Sun J, Yu Z, Wang X, Wu D. Synthesis and performance of cyclomatrix polyphosphazene derived from trispiro-cyclotriphosphazene as a halogen-free nonflammable material. ACS Sustain Chem Eng 2014;2(2):231–8.
[29] Zhang X, Xu H, Fan X. Grafting of amine-capped cross-linked polyphosphazenes onto carbon fiber surfaces: a novel coupling agent for fiber reinforced composites. RSC Adv 2014;4(24):12198–205.
[30] Gu J, Lv Z, Wu Y, Guo Y, Tian L, Qiu H, et al. Dielectric thermally conductive boron nitride/polyimide composites with outstanding thermal stabilities via in-situ polymerization-electrospinning-hot press method. Compos Part A-Appl Sci Manuf 2017;94:209–16.
[31] Chen Xa, Chen X, Zhang F, Yang Z, Huang S. One-pot hydrothermal synthesis of reduced graphene oxide/carbon nanotube/α-Ni(OH)2 composites for high performance electrochemical supercapacitor. J Power Sources 2013;243:555–61.
[32] Ma HL, Zhang HB, Hu QH, Li WJ, Jiang ZG, Yu ZZ, et al. Functionalization and reduction of graphene oxide with p-phenylene diamine for electrically conductive and thermally stable polystyrene composites. ACS Appl Mater Interfaces 2012;4(4):1948–53.
[33] Herrera-Alonso M, Abdala AA, McAllister MJ, Aksay IA, Prud'homme RK. Intercalation and stitching of graphite oxide with diaminoalkanes. Langmuir 2007;23(21):10644–9.
[34] Yue Z, Fugang X, Yujing S, Yan S, Zhiwei W, Zhuang L. Assembly of Ni(OH) 2 nanoplates on reduced graphene oxide: a two dimensional nanocomposite for enzyme-free glucose sensing. J Mater Chem 2011;21(42):16949–54.
[35] Yuan BH, Bao CL, Song L, Hong NN, Liew KM, Hu Y. Preparation of functionalized graphene oxide/polypropylene nanocomposite with significantly improved thermal stability and studies on the crystallization behavior and mechanical properties. Chem Eng J 2014;237:411–20.
[36] Zhang Y, Liu L, Sun B, Wang G, Zhang Z. Preparation of lipophilic graphene oxide derivates via a concise route and its mechanical reinforcement in thermoplastic polyurethane. Compos Sci Technol 2016;134:36–42.
[37] Gu H, Ma C, Liang C, Meng X, Gu J, Guo Z. Low loading of grafted thermoplastic polystyrene strengthened and toughened transparent epoxy composites. J Mater Chem C 2017. http://dx.doi.org/10.1039/C7TC00437K.
[38] Song S, Zhai Y, Zhang Y. Bioinspired graphene oxide/polymer nanocomposite paper with high strength, toughness, and dielectric constant. ACS Appl Mater Interfaces 2016;8(45):31264–72.
[39] Yu B, Shi YQ, Yuan BH, Qiu SL, Xing WY, Hu WZ, et al. Enhanced thermal and flame retardant properties of flame-retardant-wrapped graphene/epoxy resin nanocomposites. J Mater Chem A 2015;3(15):8034–44.
[40] Su Q, Pang S, Alijani V, Li C, Feng X, Müllen K. Composites of graphene with large aromatic molecules. Adv Mater 2009;21(31):3191–5.
[41] Vu-Bac N, Rafiee R, Zhuang X, Lahmer T, Rabczuk T. Uncertainty quantification for multiscale modeling of polymer nanocomposites with correlated parameters. Compos Part B-Eng 2015;68:446–64.
[42] Cheng HKF, Sahoo NG, Tan YP, Pan YZ, Bao HQ, Li L, et al. Poly(vinyl alcohol) nanocomposites filled with poly(vinyl alcohol)-grafted graphene oxide. ACS Appl Mater Interfaces 2012;4(5):2387–94.
[43] Gu J, Guo Y, Yang X, Liang C, Geng W, Tang L, et al. Synergistic improvement of thermal conductivities of polyphenylene sulfide composites filled with boron nitride hybrid fillers. Compos Part A-Appl Sci Manuf 2017;95:267–73.
[44] Dittrich B, Wartig KA, Hofmann D, Mulhaupt R, Schartel B. Carbon black, multiwall carbon nanotubes, expanded graphite and functionalized graphene flame retarded polypropylene nanocomposites. Polym Adv Technol 2013;24(10):916–26.
[45] Wen PY, Wang XF, Wang BB, Yuan BH, Zhou KQ, Song L, et al. One-pot synthesis of a novel s-triazine-based hyperbranched charring foaming agent and its enhancement on flame retardancy and water resistance of polypropylene. Polym Degrad Stabil 2014;110:165–74.
[46] Wang X, Xing WY, Feng XM, Yu B, Song L, Hu Y. Functionalization of graphene with grafted polyphosphamide for flame retardant epoxy composites: synthesis, flammability and mechanism. Polym Chem 2014;5(4):1145–54.
[47] Wang X, Song L, Yang HY, Lu HD, Hu Y. Synergistic effect of graphene on antidripping and fire resistance of intumescent flame retardant poly(butylene succinate) composites. Ind Eng Chem Res 2011;50(9):5376–83.
[48] Liu R, Wang X. Synthesis, characterization, thermal properties and flame retardancy of a novel nonflammable phosphazene-based epoxy resin. Polym Degrad Stabil 2009;94(4):617–24.
[49] Xing WY, Song L, Lu HD, Hu Y, Zhou S. Flame retardancy and thermal degradation of intumescent flame retardant polypropylene with MP/TPMP. Polym Adv Technol 2009;20(8):696–702.
[50] Magdas DA, Cozar O, Chis V, Ardelean I, Vedeanu N. The structural dual role of Fe2O3 in some lead-phosphate glasses. Vib Spectrosc 2008;48(2):251–4.